THE JOURNAL OF PHYSICAL CHEMISTRY A
A JOURNAL OF THE AMERICAN CHEMICAL SOCIETY

pubs.acs.org/JPCA Article

A Molecular Dynamic Study of the Effects of Surface Partitioning on the OH Radical Interactions with Solutes in Multicomponent Aqueous Aerosols

Published as part of The Journal of Physical Chemistry virtual special issue "Advances in Atmospheric Chemical and Physical Processes".

Tadini Wenyika Masaya and Fabien Goulay*

Cite This: *J. Phys. Chem. A* 2023, 127, 751−764 Read Online

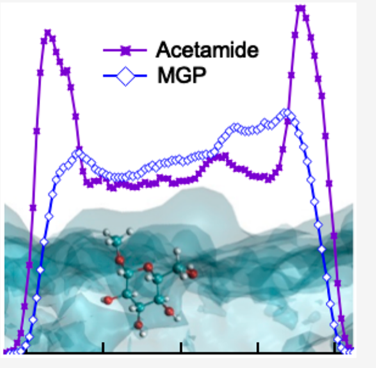

ABSTRACT: The surface−bulk partitioning of small saccharide and amide molecules in aqueous droplets was investigated using molecular dynamics. The air−particle interface was modeled using a 80 Å cubic water box containing a series of organic molecules and surrounded by gaseous OH radicals. The properties of the organic solutes within the interface and the water bulk were examined at a molecular level using density profiles and radial pair distribution functions. Molecules containing only polar functional groups such as urea and glucose are found predominantly in the water bulk, forming an exclusion layer near the water surface. Substitution of a single polar group by an alkyl group in sugars and amides leads to the migration of the molecule toward the interface. Within the first 2 nm from the water surface, surface-active solutes lose their rotational freedom and adopt a preferred orientation with the alkyl group pointing toward the surface. The different packing within the interface leads to different solvation shell structures and enhanced interaction between the organic molecules and absorbed OH radicals. The simulations provide quantitative information about the dimension, composition, and organization of the air−water interface as well as about the nonreactive interaction of the OH radicals with the organic solutes. It suggests that increased concentrations, preferred orientations, and decreased solvation near the air−water surface may lead to differences in reactivities between surface-active and surface-inactive molecules. The results are important to explain how heterogeneous oxidation mechanisms and kinetics within interfaces may differ from those of the bulk.

1. INTRODUCTION

Aqueous aerosols are known to control cloud nucleation[1−4] and to affect the climate, air quality, and human health.[5−8] A complete understanding of their role in atmospheric phenomena remains challenging as the properties of nanometric aqueous particles differ greatly from those of a bulk solution.[9−13] The chemical evolution of atmospheric aerosols as well as their ability to initiate cloud formation is mostly controlled by the properties of the gas−water interface.[2,14] Phenomena such as microconfinement,[11] high surface electric field,[15] preferred molecular orientation,[12,14,16,17] and lower water densities at the interface[18,19] affect reaction rates[10,20] and photochemical processes,[12] thus enhancing certain reaction channels while suppressing others.[21−25] Because atmospheric aerosols contain a wide range of solutes, it has become important to improve our understanding of how chemical composition changes surface reactivity.[26]

The presence of several organic compounds in aqueous aerosols results in the formation of coexisting liquid phases within the same aerosol.[27−31] In the case of water-miscible organic solutes, the core of the liquid particle, hereafter referred to as the particle bulk, acts as an infinite chemical reservoir for the outer phase. When diffusion is not the rate limiting step, thermodynamic equilibrium is reached and the composition of the air−water interface is governed by the surface−bulk partitioning properties of the solutes.[13,32,33] Surfactants with long alkyl chains have been detected in atmospheric aerosols and are known to accumulate at the surface.[3,34,35] Smaller, more hydrophilic molecules and ions also display surface−bulk partitioning leading to a solute concentration gradient close to the air−water interface.[13,36,37] Surface active molecule moves to the interface, decreasing the surface tension,[38,39] while surface inactive molecules are excluded from it, leading to an increase of the surface tension.[33] The changes in surface tension in atmospheric aerosols affect natural processes, especially cloud nuclea-

Received: October 21, 2022
Revised: December 22, 2022
Published: January 13, 2023

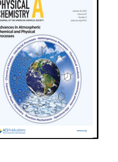

https://doi.org/10.1021/acs.jpca.2c07419
J. Phys. Chem. A 2023, 127, 751−764

tion.[40,41] A molecular-level understanding of the properties of the interface is required to fully understand the fundamental processes governing the chemical evolution of aerosols.

Surfactants at the air−water interface orient themselves with the hydrophobic chain toward the gas phase, thus forming an outer molecular layer at high concentrations.[39] Preferred molecular orientation near the air−water interface is also observed using surface-specific electronic sum frequency scattering (SFS) for smaller organic solutes such as alcohols,[42] hexafluoro-2-propanol,[43] and more recently for malachite green and propionic acid.[16,44] Molecular orientation is known to have an effect on photochemical activity[45,46] and is also likely to affect reactivity by making certain organic functional groups more or less available to surface reactive species. Although the orientation of molecules at the air−water surface may appear to be intuitive, the extent of the molecular alignment and the size of the interfacial area have been investigated only for a limited number of solutes, and their effects on reactivity remain mostly unquantified.

MD has been extensively used to investigate the orientation of molecules near the air−water interface for specific solutes at varying concentrations.[12,14,47−56] It is generally observed that alkyl groups will orient toward the surface due to their nonpolar hydrophobic nature,[57,58] with varying angles relative to the water surface.[48,52,59] For example, surface-adsorbed small brominated halomethanes are preferentially oriented with the carbon atom adsorbed on the water surface,[47,48] while halocarbons with longer nonpolar hydrocarbon chains are found to be have a parallel alignment at the water surface.[48] Similarly, acetonitrile is found to lie nearly flat at the water surface.[52,59] Ab initio quantum-mechanical molecular dynamic simulations (QM/MM) have been performed to specifically investigate the effect of solute confinements in aerosols.[12,14] The photosensitizer, imidazole-2-carboxaldehyde, is found to orient at the water surface and to have different absorption cross sections and spin orbit constants in the bulk or within the interface. Such studies highlight the strength of MD simulations for investigating interfaces as well as for explaining observed aerosol-specific chemical reactivity.

Solvation is also known to affect and modulate reactivity of organic solutes and radicals,[25,60−63] and MD simulations can provide a molecular level picture of the solvation sphere.[19,64−67] For example, the photodissociation of phenol in water has been shown to be 10^4 faster at the water surface than in the bulk.[18] Recent MD simulations coupled to quantum calculations showed that the interfacial process is accelerated due to a lower dissociation barrier from incomplete hydrogen bonding to phenol at the air−water interface.[19] Water is also shown to stabilize the transition state for abstraction of a hydrogen atom from a solute leading to faster reaction compared to nonpolar solvents.[62] Interfacial solvation and molecular orientations are difficult to probe experimentally, especially because SFS techniques remain insensitive to molecules with lower surface density and higher orientational disorder.[42] Classical and ab initio MD methods are therefore required to gain the required molecular-level understanding of the surface properties.

In the atmosphere, the OH radical is one of the most abundant oxidizer.[68] MD simulations have shown that the radical absorbs at the water surface and partitions between the bulk and the surface with an enhanced surface concentration.[69−74] The preference of the OH radical for the air−water interface can be compared to the radical predicted diffusion−reaction length (∼1−2 nm)[75−78] under reactive conditions. Both suggest that the initiation step of the heterogeneous oxidation predominantly takes place within the interface. Several studies have also looked at the solvation of the OH radical.[62,63,79−85] A different solvation of the radical and solute near the interface could explain enhanced surface rate coefficients[24] and changes in oxidative chemical scheme. Overall, the reaction within the air−water interface will be governed by an interplay of the solute concentration gradients, the reactant solvation, and the molecular orientations. For all these reasons, surface active molecules are more likely to react with the OH radical while surface inactive molecules may be shielded from oxidation. A better understanding of the chemical evolution of multicomponent aqueous aerosols under atmospheric conditions therefore requires a systematic study of the behavior of a wide range of molecules within the air−water interface.

Atmospheric aerosols contain a wide range of solutes with different organic functional groups. In multicomponent particles, even though the solutes are dilute enough to neglect intermolecular interactions, concentration gradients near the surface lead to solute reactive uptake coefficients that are different from those observed in a single component particle.[32] A better understanding of the effect of composition on the chemical fate of aerosols under oxidative conditions therefore requires a systematic investigation of the effect of the organic functional groups on heterogeneous reactivity. Amides and saccharides are good archetypal molecules for investigating such effects as they display a very wide range of partitioning properties. Table 1 displays the chemical structures of a series

Table 1. Names, Structures, and Partition Coefficients for the Organic Solutes Used in the MD Studies

Molecule	Chemical structure	K_p[33]
β-D-glucose	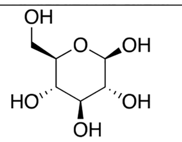	0.2
Methyl β-D-glucopyranoside (MGP)	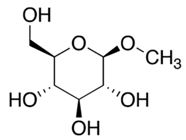	
Urea	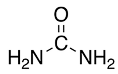	0.8
Acetamide	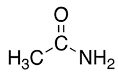	3.7
Propionamide	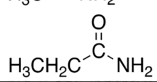	

of amides and saccharides. When available, it also displays the partition coefficient K_p.[13,33] A value lower than unity is characteristic of a surface inactive molecule with a preference for the water bulk. The concentration of the solute near the water surface is quasi-null for K_p close to 0[13,33] and increases as K_p increases. Glucose, methyl β-D-glucopyranoside (MGP), and urea are considered as surface inactive, while acetamide and propionamide are surface active. The solvation of amides has been extensively studied both experimentally by means of

https://doi.org/10.1021/acs.jpca.2c07419
J. Phys. Chem. A 2023, 127, 751−764

various spectroscopic techniques[8,86−100] and theoretically by Monte Carlo simulations[101,102] and MD methods.[103−111] The hydrophobic and hydrophilic nature of amides influences the amide−water interaction and the properties of the water solvation shells around the molecule.[112−115] Similarly, there are a large number of studies on the solvation of saccharides showing their preference for the water phase.[116−122] Although sugars are not expected to partition toward the surface, they were suggested to have an enhanced reactivity toward phosphorylation at the air−water interface of microdroplets.[17] A more systematic investigation of organic solute behavior at the interface is therefore required to fully discriminate between surface reactivity and other competing processes.[123,124]

In this study, classical MD is used to investigate the surface properties of series of saccharides and amides (see Table 1), as well as their effect on the OH−solute interaction near the surface. The interface of aqueous particles is simulated using a 80 Å cubic water box surrounded by OH radicals in the gas phase. Although the model is oversimplistic and does not include reactive interactions, it still provides molecular-level information about the solutes' surface properties and radical−solute interactions. The size of the simulation box allows for the comparison of the solute behaviors between the bulk and the interface as well as the sizing of the interfacial region. Surface active molecules are found to migrate to the interface and to systematically orient with the alkyl group pointing toward the water surface. The molecules regain full rotational freedom 2 nm away from the surface. The structure of the solvation sphere is also found to change considerably at the interface. Glucose and urea are confined to the bulk with no preferred orientation. MGP is found to be amphipathic with low surface concentration but still adopting a preferred orientation near the surface. The concertation gradient, the molecular orientation, and the tighter OH−solute interactions near the surface all suggest a different reactivity when molecules are confined to the interface. The computational study establishes trends to better understand the different of reactivity observed in multicomponent aqueous particles. The results, together with known bulk reaction mechanisms for saccharides and amides,[125−128] are used to discuss the OH-initiated oxidation of particles containing several solutes with different partitioning properties.

2. METHODS

2.1. Molecular Dynamics. The simulation method and model setup are taken from previous studies on similar systems.[52,69] The air−particle interface was modeled using a 80 × 80 × 80 Å^3 simulation box filled with 13 333 water molecules and 14 or 240 organic molecules. This corresponds to a nominal solute mole fraction of 1.0×10^{-3} or 18×10^{-3} (concentrations of 0.06 or 1.0 mol L^{-1}, respectively). The water box was surrounded on both sides along the z-axis by 80 Å vacuum boxes filled with a total of 40 OH radicals (see Figure 1), resulting in an overall 80 × 80 × 240 Å^3 system.[129,130] The OH radical mole fraction is 0.003, which is twice lower than that used in previous MD investigations.[69] Vacuum was used instead of air as the number of nitrogen and oxygen molecules would be negligible within the considered volume.[129,131] This volume is hereafter referred to as air. The 240 organic molecules in the water box were made up of urea, glucose, methyl β-D-glucopyranoside (MGP), propionamide, or acetamide. Solute mixtures were also investigated using an equal number of either urea and MGP, propionamide and acetamide, or acetamide and MGP. Water was modeled with the rigid three-charge three-site TIP3P model including Lennard-Jones interaction on all atoms.[132,133] The OH radical model was based on previous models available in the literature.[69] The OH radical permanent dipole was modeled using a −0.32e partial charge on the oxygen atom and a +0.32e partial charge on the hydrogen, with e the elementary charge. The O−H bond length was set to 0.97 Å and the bond energy to 545 kcal mol^{-1} Å^{-2}. The Lennard-Jones parameters on the atoms were adopted from the hydroxide ion model.[69,134] The urea, propionamide, and acetamide geometry and interaction parameters were taken from the CHARMM 36 force field. In the case of MGP these parameters were adopted from D-glucose with methyl patch parameters from the CHARMM 36 force field.[135,136] Nonbonding forces used a cutoff of 12 Å, and electrostatic interactions were modeled using the particle mesh Ewald method.[137,138] All simulations were performed using the NAMD 2 package, version 2.14.[139]

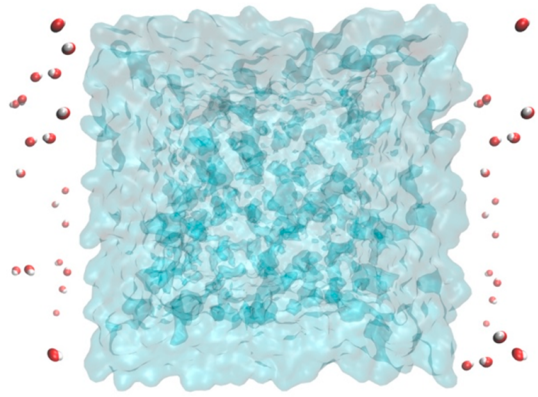

Figure 1. Initial water-box configuration of the constant NVT simulation cell.

The organic molecules were randomly placed in the simulation box using PACKMOL[140] followed by the OH radicals on either side of the box periodic boundary conditions. The water molecules were added last to the simulation box using the VMD program solvation plugin.[141] A constant NPT (constant number of particles, pressure, and temperature) preliminary run with 5000 minimization steps was run first with a 1 fs time step. The pressure and temperature were kept constant at 1 atm and 298 K, respectively, using a Langevin barostat and thermostat with the damping coefficient set to 1/ps.[142] During this initial simulation, the hydroxide radicals were held in fixed positions using fixed atom parameters.

The initial production run outcome from the NPT ensemble was used as the starting point for the final NVT ensemble (constant number of particles, volume, and temperature). A constant-NVT equilibration run was performed for 5 ns, followed by a 110 ns constant-NVT production run, all with a time step of 1 fs. The constraints on the OH radicals from the initial production run were removed, and lateral pressure calculation parameters were added to enable the calculation of surface tension.[129,143] Five independent production runs with different organic molecule initial coordinates were performed to account for the effect of starting conformations on the final simulation results. Figure S1 displays the bulk and interfacial mole fractions of MGP and acetamide as a function of simulation time. The constant mole fractions at long time are evidence that the simulation has converged. The data displayed

https://doi.org/10.1021/acs.jpca.2c07419
J. Phys. Chem. A 2023, 127, 751−764

Table 2. Simulated and Experimental Water Bulk Diffusion Coefficients (D) and Specific Density (ρ) at Different Temperatures (T) and Total Number of Water Molecules Used in the Simulations (N)

method	ref	T (K)	D (10^{-9} m^2 s^{-1})	ρ (g cm^{-3})	N
TIP3P	Present study	298	4.91(0.21)	0.998	13676
TIP3P	van der Spoel et al.[149]	301(4.4)	5.40(0.14)	1.001	820
TIP3P	Mark and Nilsson[150]	297.0(0.9)	5.60(0.08)	0.998	901
TIP3P	Mahoney and Jorgensen[151]	298.15	5.19(0.08)	0.993	267
TIP3P	Wu et al.[152]	298.16	5.30	0.986	216
TIP3P	Vega and De Miguel[153]	298	5.51		360
TIP3P	Wang and Hou[154]	298	2.98		624
TIP3P	Leontyev and Stuchebrukhov[155]	298.15	6.10	0.9986	2048
TIP3P	Chen et al.[156]	298.15	5.06		256
TIP3P	Yu et al.[157]	298.15	6.14	1.008	2100
TIP3P	Braun et al.[158]	298.15	5.50	0.98	
Exp	Holz et al.[159]	298	2.30		
Exp	Price and Brooks[160]	298		0.997	

Table 3. Comparison of Simulated and Experimental Water Oxygen−Oxygen and Oxygen−Hydrogen Pair Distribution Functions (g)

	Oxygen−Oxygen						
	ref	first maximum		second maximum		third maximum	
method	oxygen−oxygen	position (Å)	g_{OO}	position (Å)	g_{OO}	position (Å)	g_{OO}
TIP3P	Present study	2.75	2.68	4.55	1.00	6.85	1.02
TIP3P	Mark and Nilsson[150]	2.77	2.67	4.50	0.99	6.84	1.02
Exp	Soper and Phillips[162]	2.88	3.09	4.50	1.14	6.73	1.07

	Oxygen−Hydrogen				
	ref	first maximum		second maximum	
method	oxygen−hydrogen	position (Å)	g_{OH}	position (Å)	g_{OH}
TIP3P	Present study	1.85	1.27	3.25	1.44
TIP3P	Mark and Nilsson[150]	1.83	1.24	3.22	1.44
Exp	Soper and Phillips[162]	1.85	1.38	3.30	1.60

below are from a single production run and are representative of the outcomes of all five independent runs.

2.2. Data analysis. Density profiles ρ of a species along the z-axis were determined using the density profile tool in the VMD program.[144] The modeled volume was divided into equally sized slabs along the z axis of thickness Δz. The density profile of a property p_i for an atom indexed i was calculated using eq 1:

$$\rho_n = (L_x L_y \Delta z)^{-1} \sum_{\text{atom } i} \delta_n(z_i) p_i \qquad (1)$$

where n is the slab integer, L_x and L_y are the sides of the periodic cell, and $\delta_n(z_i)$ is the indicator function which is unity if the coordinate z_i is within the slab volume and zero otherwise.[144]

Radial pair distribution functions (RDF) $g(r)$ were calculated using the RDF tool in VMD. The tool calculates the spherical atomic radial distribution function $g(r)$ between the coordinates of two selected atoms over a given trajectory. The RDF calculations are performed within the full simulation box as well as within the liquid bulk center and the interfacial regions.[145] RDFs for each atom and molecule pair are histogrammed into 240 bins from a distance 0−24 Å (twice the maximum force cut off distance). The RDFs between different atom pairs and molecule pairs give a depiction of molecular arrangements and microstructure in the different regions of our simulation.

Surface tension values γ were calculated using the mechanical definition of the atomic pressure. Surface tension is defined in terms of the difference between the normal (z-direction) and lateral components of the pressure tensor. For this study in which a simulation cell of length L_Z (=3L) contains two surfaces, γ can be expressed using eq 2:

$$\gamma = \frac{1}{2}\int_0^{L_Z} [P_{ZZ} - 0.5(P_{XX} + P_{YY})]\, dz \qquad (2)$$

where P_{XX}, P_{YY}, and P_{ZZ} are the three diagonal components of the pressure tensor along the x, y, and $z$directions, respectively.[129]

3. MODEL VALIDATION

The validity of the model to predict the behavior of organic molecules at the air−water interface was verified by calculating self-diffusion coefficients and the bulk water density, examining water and OH radial density functions, and examining trends in calculated surface tensions. All the results presented below are for a nominal solute mole fraction of 18 × 10^{-3}. The self-diffusion coefficients D of water and glucose were estimated from mean square displacement (MSD) using Einstein's relation:[146]

$$D = \lim_{t\to\infty} \frac{\langle [r(t) - r(0)]^2 \rangle}{6t} \qquad (3)$$

https://doi.org/10.1021/acs.jpca.2c07419
J. Phys. Chem. A 2023, 127, 751−764

Table 4. Positions of the Water−OH Radial Density Profile Maxima

atoms	first maximum (Å) present study	first maximum (Å) Campo and Grigera[163]	second maximum (Å) resent study	second maximum (Å) Campo and Grigera[163]
H* H	2.45	2.4	4.45	4.30
H* O	1.75	1.75	3.75	3.75
O* H	2.05	1.97	3.35	3.35
O* O	2.85	2.85		6.90

where t is time, and $[r(t) - r(0)\ ]^2$ is the mean square displacement.[147] The bulk density ρ of water is calculated using the following relation:

$$\langle \rho \rangle = \frac{M n_{res}}{N_{avo} \langle V \rangle}$$

were M is molar mass of water, N_{avo} is the Avogadro number, n_{res} is number of water residues in the box of interest, and $\langle V \rangle$ is the average simulation box volume.[148]

Table 2 displays calculated and measured diffusion coefficients and water densities from the present study and previous studies on aqueous systems. The self-diffusion coefficient and water density from the present study compares well to literature values from the TIP3P water model.

The water distribution functions, $g_{OO}(r)$, $g_{OH}(r)$, and $g_{HH}(r)$ were calculated and compared to literature data on similar systems (Table 3). The results from this study compare reasonably well to other simulations and experimental results. The RDF between oxygen−oxygen pairs of two water molecules (Figure S2) is similar to literature profiles[129] and shows a sharp peak at 2.75 Å (Table 3) for all three simulation setups. This value is close to the expected average hydrogen bond length in water, 2.8 Å.[161] In addition, all RDFs between two identical species (not showed) are found to be independent of the particle composition as expected for such dilute systems.

The RDFs of water atoms around the OH radical in the system were calculated and compared to literature profiles. Table 4 displays the peak positions for the different atoms. The present simulations are in good agreement with Campo and Grigera.[163]

The surface tension of pure water is calculated to be 75.3 mN/m, 5% higher than the experimental value.[129] Although MD has been extensively used to model the air−water interface,[129] calculated surface-tension values vary considerably even for studies using the same water model. The discrepancy is due to different simulation parameters and even simulation times.[129] The goal of the surface tension calculations performed here is to examine the relative change in value due to the addition of solutes. Table 5 shows the simulated values of surface tension obtained for different solutes and solute mixtures. As solutes are added to the water system, the calculated surface tension decreases. Amides are known to greatly reduce the air−water surface tension[33,164] with an expected increasing effect as the alkyl chain length increases. Urea has been measured to increase the water surface tension, although the effect is expected to be negligible at the solute concentrations used in the simulations.[33,165] Similarly, the addition of sugars to water, at low solute concentrations, is expected to lead to a negligible change.[166] The very small decrease of surface tension after addition of urea or glucose observed in Table 5 compared to pure water is likely to be an artifact of the modeling. The presence of a methyl group in MGP reduces its hydrophilicity compared to glucose and induces a measurable decrease of the surface tension. Overall, as seen in Table 5, the addition of an alkyl group to the solute consistently decreases the air−water surface tension.

Table 5. Simulated Surface Tension Values for Air−Water Interfaces Containing Different Solutes and OH Radicals

solutes	surface tension (mN/m)	solutes	surface tension (mN/m)
Glucose	72.8	MGP and urea	66.5
Urea	71.5	MGP and acetamide	63.4
MGP	67.9	Propionamide and acetamide	56.6
Acetamide	67.5		
Propionamide	58.5		

Figure 2 displays the OH radical profiles for the three different mixtures. The origin of the z-axis is located 40 Å before the center of mass of the water box and is defined as the water surface. For all simulations, OH radicals maintain similar density distributions regardless of the combination of molecules making up the multicomponent system. The OH density profiles show an increase in density from a constant value in the gas phase (with less than 5% fluctuation) to maxima near the water surface, followed by a sharp drop and a constant value within the water bulk. The density profile is characteristic of the radical preference for the air−water interface. During the last 50 ns of the simulation (Figure S3), one OH radical spends an average of 45% of the simulation time within the first 10 Å below the surface, 24% in the gas phase, and the remaining 31% in the bulk. Hydroxyl radicals being predominantly located at the interfacial regions agrees with the findings of Roeselová et al.[69] as well as with the potentials of mean force (PMF) calculations by Vácha and Slavíček et al.[70] showing active uptake of OH radicals at the interface.

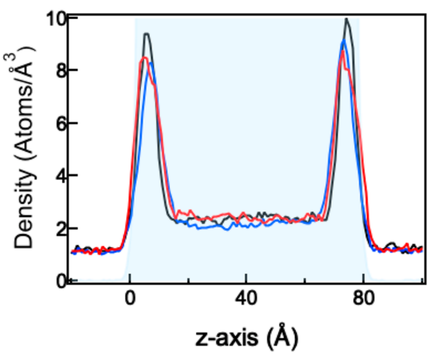

Figure 2. OH radical density profiles for a MGP−urea mixture (black line), acetamide−propionamide (blue line), and acetamide−MGP (red line) across the water box (blue shaded area).

https://doi.org/10.1021/acs.jpca.2c07419
J. Phys. Chem. A 2023, 127, 751−764

Figure 3 displays the scattering plot of one OH radical (black dots) within the last 7 ns of the simulation. It shows occurrences of adsorption (green), desorption (red), absorption (purple), and transfer from the bulk to the interface (dark blue). In the absence of reactions, the radicals are at a dynamic equilibrium between the different phases of the system. These results are consistent with previous MD simulations of OH interaction at the air−water interface,[69,167] although performed here over a much longer simulation time.

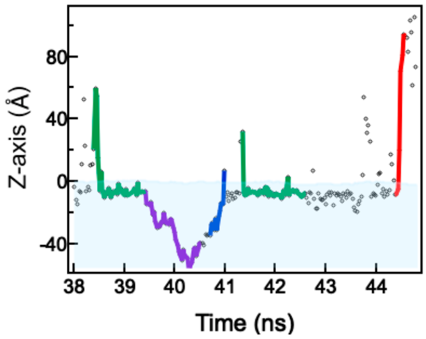

Figure 3. Scattering plot of one OH radical (black dots) within the last 7 ns of the simulation. Different trajectories of the radical are highlighted: gas−surface adsorption (green), desorption (red), absorption (purple), and bulk-to-interface transfer (dark blue). The blue shaded area is the water box.

4. RESULTS AND DISCUSSION

Following the simulation, all organic molecules are found to be confined to the water box. Water evaporation is found to occur with a rate of 0.24 molecules nm^{-1} ns^{-1} which is higher than previous studies.[168] Nonetheless, evaporation does not significantly change the dimension of the system during the simulation time. The air−water interface is defined to extend 10 Å into the water box and 10 Å into the gas phase. The interface may also be defined as the region where the water density is between 10% and 90% of its bulk value.[167] Because no solute molecules were found in the gas phase, the two definitions lead to similar results. The following sections present MD simulation results for water systems containing mixtures of saccharide and amide molecules. The data are interpreted using literature findings and discussed with special attention to surface concentration gradients, molecular alignment, and OH−solute interactions. All the results presented below are for a nominal mole fraction of 18×10^{-3}.

4.1. Surface Concentration Gradients. The propensity of a molecule to be confined to the interface may be determined by inspecting the density profiles along the simulation box axis. Figure 4 displays density profiles of (a) MGP and urea, (b) acetamide and propionamide, and (c) MGP and acetamide mixtures along the z-axis of the simulation box. The water box is represented by the blue shaded area and the interface by the purple shaded area. In Figure 4a, the density profiles of the two organic species (urea and MGP) show an increase from zero at the liquid surface to respective maxima within the water bulk or within the air−water interface. In the bulk phase, the density fluctuations are less than 20% from the maximum value. In the case of urea, the lack of a maxima within the interface area and near-flat density profile in the bulk indicate that the organic species has a higher preference for the liquid bulk. The MGP density profiles

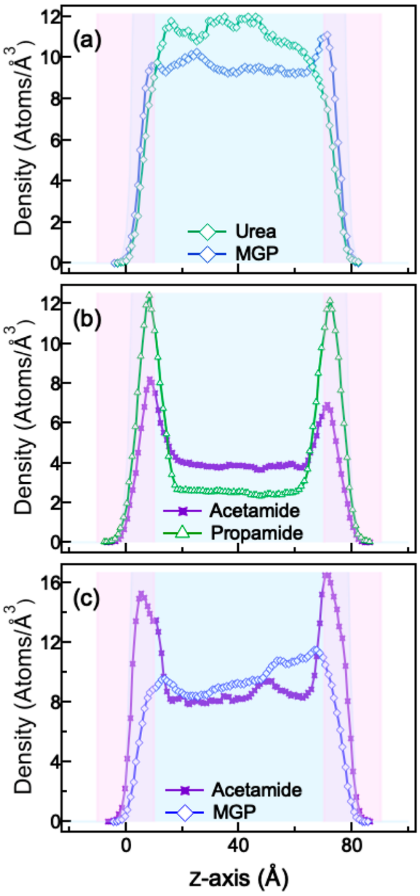

Figure 4. Density profiles of (a) MGPL (blue open diamonds) and urea (green filled diamonds), (b) acetamide (purple starts) and propionamide (open green triangles), and (c) acetamide (purple stars) and MGP (blue open diamonds) across the water bulk (blue shaded area), air−water interface (purple shaded area), and air (unshaded area).

(Figure 4a and Figure 4c) display a sharper density rise than that of urea within the interfacial area, although most of the molecules remain located within the bulk. The affinity of an organic molecule for a given region may be quantified by integrating the density profile over the corresponding z-range. For reference, the water volume within the interface represents 25% of the total water box. The integrated profile values are given in Table 6. With a relative bulk value of 89% for urea and 84% for MGP, MGP has a slightly higher affinity for the interface than urea.

In Figure 4b, the density profiles of propionamide and acetamide show a sharp increase with maxima within the interface. The bulk density is found to be much lower than that

Table 6. Integrated Density Profiles (% of Total Area)[a]

molecules	interface (%)	bulk area (%)
MGP	16	84
Urea	11	89
Acetamide	28	72
Propionamide	45	55
MGP	17	83
Acetamide	33	67

[a]The interface values are the sum of the left and right interfaces.

https://doi.org/10.1021/acs.jpca.2c07419
J. Phys. Chem. A 2023, 127, 751−764

of urea and MGP (Figure 4a). The propionamide density profile displays a sharper density rise within the interfacial region compared to that of acetamide, resulting in 45% of the propionamide molecules within the interface compared to 28% for acetamide (see Table 6). The trends described in Figure 4a,b for MGP and acetamide are also observed in Figure 4c for a mixture of MGP and acetamide. In all cases, in Figure 4, within the fluctuations of the models, the density profile of a given molecule is found to be independent of the chemical composition.

The shapes of the profiles observed for urea and MGP in Figure 4 are likely due to the amphipathic properties of MGP and the strictly hydrophilic nature of urea. Urea possesses only polar functional groups, two NH_2 groups, and one carbonyl group, all contributing to its hydrophilicity and overall bulk preference. MGP possesses polar functional groups (hydroxyl group) and one nonpolar functional group (methyl). The polar functional groups contribute to its hydrophilic tendency resulting in bulk preference, but the presence of one methyl group in MGP induces a change that reduces the molecule's hydrophilicity. The effect of the methyl group is apparent when comparing the density profiles of MGP and D-glucose (Figure S4). In the cases of acetamide and propionamide, the hydrophobicity of the alkyl functional group is known to increase with increasing chain length,[112−115] leading to a distinct propionamide preference for the interface.

For all the investigated solutes, the bulk concentration is achieved within 2 nm from the water surface. For surface-active molecules this results in the formation of a thin layer with concentrations higher than that of the bulk. Similar surface-enhanced concentrations have been observed for aqueous particles containing ionic solutes.[36,37] In this case the thickness of the surface excess charge layer ranges from 1.4 to 2 nm depending on the ion structure and is independent of the particle size. The similarities between the two systems suggest that the thickness of the partitioning layer is a property of the solvent and may be independent of the solute. Although not investigated here, the thickness of the partitioning layer is likely to also be independent of the particle size. For larger particles (>1 μm), any interfacial phenomena would therefore also occur within a similar 2 nm layer. Even though the fraction of the interface volume to that of the particle decreases with increasing particle radius, the properties of this layer may be sufficient to considerably change chemical mechanisms in microdroplets.[15,17]

The effect on concentration on the density profiles was investigated by running the simulations at two different solute mole fractions. Figure S5 displays the density profile of acetamide at mole fractions of 1.0×10^{-3} and 18×10^{-3}. The profile shape is similar in both cases. The fraction of acetamide within the interface is 37% at 1.0×10^{-3} compared to 33% at 18×10^{-3}. In both cases, the profiles reach their bulk concentration within ~2 nm of the water surface. At the low solute fractions used in the simulations, concentration has no significant effect on the solute density profiles. This finding agrees with previous investigations about the effect of concentration on surface confinement performed at much higher mole fractions.[49,52,59]

4.2. Molecular Orientation at the Interface. Density profiles for individual functional groups of a given solute are used to investigate molecular orientation as a function of distance from the surface. Figure 5 displays the atom density profiles for (a) MGP, (b) acetamide, and (c) propionamide along the *z*-axis. The MGP carbon labeling is displayed in Figure S6. For all three molecules, the density profiles of the methyl group (black lines) are shifted toward the surface compared to that of the other functional groups. In the water bulk, all profiles are indistinguishable. The atom density profiles for both urea and glucose (Figure S7) are indistinguishable within the interface and the bulk.

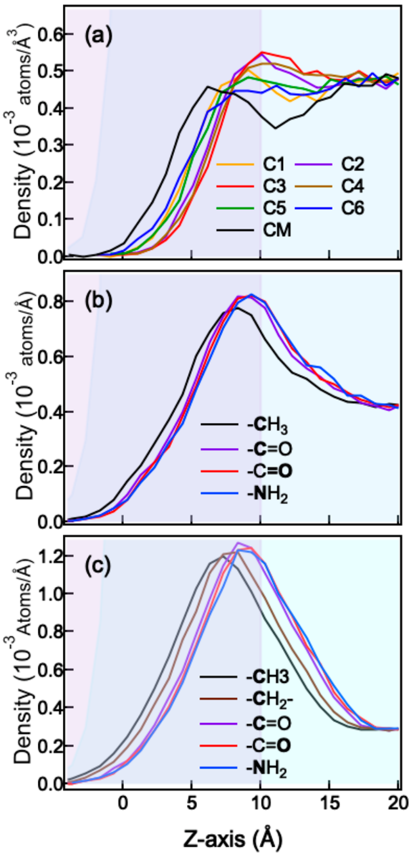

Figure 5. Atom density profiles for (a) MGP, (b) acetamide, and (c) propionamide across the water bulk (turquoise blue) and air−water interface (purple) interface.

The atom density distribution profiles for MGP, acetamide, and propionamide displayed in Figure 5 all suggest that the molecules loose rotational freedom near the surface and adopt a preferred orientation with the most hydrophobic group pointing toward the water surface. Molecules recover full rotational freedom 2 nm away from the surface. No preferred orientation is observed at the interface for urea and glucose. The preferred orientation of the molecules at the interface is consistent with previous findings for alkanes and acetonitrile.[52,114] The orientation adopted by the acetamide, propionamide, and MGP are attributed to nonpolar hydrophobic nature of the methyl functional group.[57,58] Figure 6 is a snapshot of the interface showing the MGP preferred orientation with the methyl group pointing toward the surface.

The expected OH reaction mechanism with saturated organic solutes is fast abstraction of a H atom from the molecule to from a radical and a water molecule.[125,126] Further reaction with molecular oxygen leads to peroxy radicals which decompose to give carbonyl molecule and HO_2 radicals.[127] In the bulk phase, the abstraction of the H atom from the different sites of MGP has been shown to follow a statistical distribution with a near 3:2:1 ratio for abstraction from the

https://doi.org/10.1021/acs.jpca.2c07419
J. Phys. Chem. A 2023, 127, 751−764

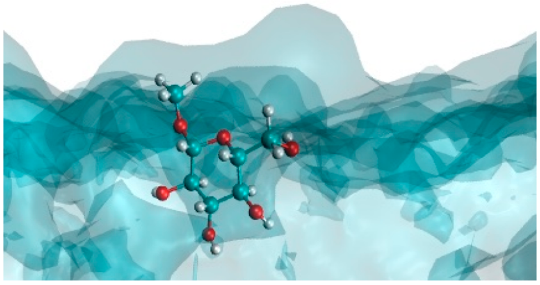

Figure 6. Snapshot of the air−water interface showing an oriented methyl β-D-glucopyranoside molecule.

Table 7. Number of Molecules Sampled around Different Solutes within the Bulk or the Air−Water Interface[a]

	bulk		interface	
	H_2O	OH·	H_2O	OH·
OH radical (4.25 Å)	15.3		4.5	
OH radical (2.45 Å)	3.3		1.5	
Acetamide (4.25 Å)	27.4	0	15.4	0.3
Urea (4.30 Å)	23.7	0	15.2	0.1
Glucose (4.30 Å)	35.3	0	29.8	0.1
MGP (4.30 Å)	38.4	0	30.6	0.1

[a]The number in parentheses indicates the cutoff distance for determination of the solvation sphere.

methyl group, ethyl group, and any other carbon sites, respectively.[126] The preferred MGP orientation displayed in Figure 6 leads to the methyl groups becoming more accessible for reactions with gaseous and adsorbed species such as the OH radical. It is likely that within the interface the H-abstraction process is no longer statistical. Because each abstraction reaction product has a different reactivity toward O_2, product distributions for the OH-initiated oxidation of MGP in aerosols will differ from that of the bulk. The effect is likely to be even more pronounced in the case of propionamide as more molecules will be confined to the interface. In the bulk, the abstraction rates from the amide alkyl chain are estimated to be twice as fast as that from the $-NH_2$ group.[127] Abstraction in α position from the amide group is favored due to radical stabilization. Upon migrating to the interface, the molecule will orient with the alkyl group facing the water surface, likely further favoring abstraction of the alkyl hydrogens relative to those of the $-NH_2$ group.

Preferred molecular orientation of glucose at interfaces was suggested by Zare and co-workers[17] to explain the production of sugar phosphates in charged microdroplets. The atomic density profiles for glucose (see Figure S7), however, shows no preferential orientation of the molecule near the water surface. Combined with glucose preference for the particle bulk, it is unlikely that interfacial orientation contributes to spontaneous phosphorylation. Gas phase reactions may instead be responsible for the observed enhanced chemistry.[123,124]

4.3. Interfacial Solvation and OH−Solute Interactions. Although the MD simulations do not include reactive interactions, information about how confinement at the interface affects the chemistry may be inferred from inspecting the interaction between solutes and solvent molecules. The structures of the solute solvation shells were obtained by probing the instantaneous configurations of each solute at every time step (>100 frames) of the MD trajectories. The water molecules included in the solvation sphere were determined based on the distance between the water oxygen atom to any of the carbon atoms of the solute. The cutoff distance corresponds to the first local minima of the oxygen−solute radical distribution functions.[64,67] Similar instantaneous configurations of OH radical−solute positions were also sampled. The number of OH radicals around the solutes was determined based on the distance of the radical oxygen atom to any one of the carbon atoms of the solutes.

Table 7 displays the number of water or OH molecules around the different solutes in the bulk or within the interface. The values displayed in Table 7 for OH are without any other solutes. The solvation shell of the OH radical is found to vary by up to 10% (not shown) depending on the solutes present in the water box. The change in functional group in the solute does not have large effects on the solvation sphere as observed for other systems.[64−66] The hydration shell for surface active solutes and the OH radical is found to decrease considerably at the interface. Similar "half-hydration" has been observed for molecules such as coumarin 110.[110] The change is less significant for glucose and MGP, although in the case of methyl substituted sugar, the lower hydration shell is consistent with the alignment of the methyl group toward the surface.

Radial pair distribution functions (RDFs) $g(r)$ were plotted to quantify the interaction between the OH radical and the different functional groups of the organic solutes in both the interface and the bulk regions. Figure 7 displays the RDFs of the OH radical H atom with the carbonyl oxygen atom of (a) urea, (b) acetamide, and (c) propionamide in the bulk (red lines) and at the air−water interface (blue lines). RDFs for the interaction of the OH radical with the other atoms are displayed in Figure S8. In Figure 7 the RDFs display two maxima, one for distances below 3 Å and one for longer distances. The sharp peak at short distances is characteristic of hydrogen bonding interactions between the radical H atom and the carbonyl oxygen. For all three molecules, within the interface, this peak is more intense than the second broader peak. Its intensity decreases within the bulk and, in the case of propionamide, becomes very small compared to that of the broader peak. A similar difference between RDFs in the bulk and interface is observed for the carbonyl carbon (Figure S9). Bulk and interface RDFs display similar features at both mole fractions investigated here (see Figure S9 for the lowest mole fraction RDF of propionamide). Radical distribution functions in the interface also appear to decay faster with r than those in the bulk. This suggests a tighter interaction between the OH radical and the organic solute within the interface. This is likely due to the different molecular packing and solvation at the interface relatively to the bulk.

According to the mobility mechanism of the OH radical in solution[63] and because of the lower solvation sphere, the encounter of the solutes with the radical will take less steps at the interface than in the bulk. This is evidenced in Table 7 by the higher number of OH radical penetrating the solute solvation shell within the interface compared to the bulk. Other solvation effects, such as stabilization of the transition states and intermediates, need to be investigated to fully understand how the interfacial solvation may affect the reactivity. Although such interactions may not be representative of the reactive potential between the radical and the molecule, they provide valuable information to understand surface phenomena in aqueous aerosols.

https://doi.org/10.1021/acs.jpca.2c07419
J. Phys. Chem. A 2023, 127, 751−764

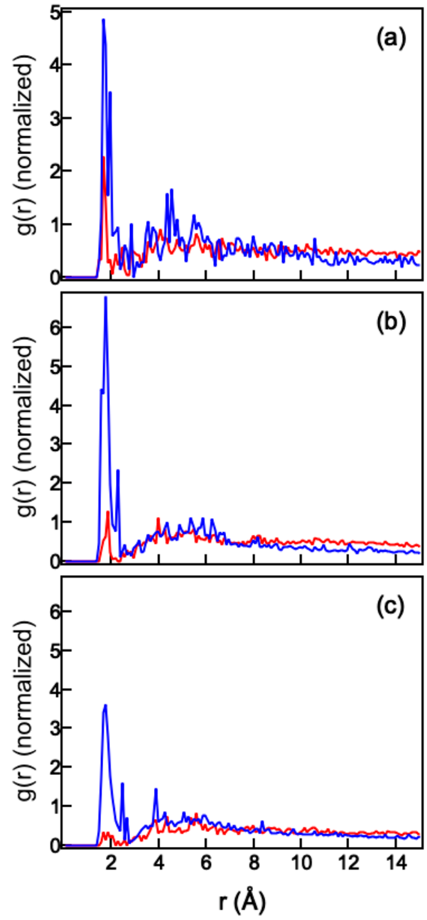

Figure 7. Radial pair distribution functions of the OH radical H atom with the carbonyl oxygen atom for (a) urea, (b) acetamide, and (c) propionamide in the bulk (red lines) and at the air−water interface (blue lines). The profiles are normalized by the area under the curve.

5. CONCLUSIONS AND IMPLICATIONS FOR ATMOSPHERIC HETEROGENEOUS CHEMISTRY

The MD simulations described above provide a molecular level snapshot of the air−water interface as found in atmospheric multicomponent aqueous droplets. Analysis of the density profiles and radial distribution functions for saccharide and amide solutes as well as for OH radicals provides quantitative information about the dimension and composition of the interface and shows how molecular structure governs the behavior of these solutes near the water surface. Although it does not model the whole droplet, the simulations show that for the systems investigated here:

(1) Bulk properties are reached within the first 2 nm of the surface. Surface active molecules, such as propionamide and acetamide, are found to accumulate within the top 2 nm of the droplet, while surface inactive molecules, such as urea and glucose, form a depletion zone at the surface. For a particle containing a mixture of urea and acetamide, the properties of the outer phase are solely defined by acetamide, while those of the inner phase are mostly defined by urea. The MD simulations also confirm that the OH radicals preferentially accumulate within the 2 nm interfacial region. The dimension of the interface is comparable to the diffusion−reaction length (∼1−2 nm)[75−78] of the radical under reactive conditions. This overlap is likely to lead to interface-specific reaction mechanisms and kinetics. For aqueous aerosol for which diffusion of the reactants to the surface is not the rate limiting step, surface active molecules are rapidly consumed while surface inactive molecules are shielded from direct reaction with the oxidant.[13]

(2) Surface active solutes lose rotational freedom and orient themselves with the hydrophobic group pointing toward the water surface. Methyl-substituted glucose is mostly surface inactive with low surface concentrations but still displays a preferred surface orientation due to the presence of a methyl group. Hydrophobic organic groups will become more accessible for reaction, changing the likely reaction mechanism compared to that of the bulk. Such behavior is expected for a surfactant with large alkyl chains and is shown to happen here for substituted saccharides and amides.

(3) Reduced OH radical and solute solvation at the interface leads to an increased number of OH radicals coming into contact with the investigated surface-active solutes. As expected, the number of water molecules in the radical and solutes solvation spheres is found to decrease considerably within the interface. The extent of this decrease depends on the molecular structure. This leads to a tighter interaction between the OH radical and the organic solute within the interface as observed in the radial pair distribution functions. The effects will contribute to a change in reaction rate coefficients within the interface compared to the bulk.

The increased surface concentration, molecular orientation, and tighter OH−solute interaction all suggest a different reactivity of surface-active molecule within the air−water interface compared to bulk molecules. These findings have major implications for the chemical transformation of aqueous aerosols where the interface is a gateway for atmospheric oxidizers. The different surface behavior of the organic solutes can explain heterogeneous atmospheric phenomena that are inconsistent with known bulk liquid or gas phase chemistry.[15,17,19,169]

Amides and urea[170] as well as saccharides[171] have been detected in atmospheric aerosols at concentrations much lower than that used in the modeled system. Density profiles and the extent of the molecular alignment are expected to change with solute concentrations.[49,52,59] In the cases of a water−acetonitrile[52,59] and water−dimethyl sulfoxide the systems displays solute enhancement at the air−water surface for mole fractions up to 0.20 with a surface peak concentration that decreases with increasing solute mole fraction. At higher mole fractions, although the solute profiles may not display a significant surface enhancement, the surface concentration remains greater than that of the bulk. This trend suggests that surface concentration enhancement is still expected at solute mole fractions lower than that used in the present study (0.0018). In addition, the width of the high-concentration region is found to be relatively independent of the solute mole fraction.[52] The interface properties observed here for saccharides and amides are therefore likely to remain relevant at the low solute mole fractions found in atmospheric aerosols.

In mixed particles, urea will be shielded from reaction with OH by surrounding surface active compounds. In the gas phase, amides react with the OH radical through abstraction of a hydrogen atom from the alkyl group, with negligible

https://doi.org/10.1021/acs.jpca.2c07419
J. Phys. Chem. A 2023, 127, 751−764

abstraction from the NH_2 group.[172] Although the overall gas phase rate coefficients are relatively low ($<2 \times 10^{-12}$ cm^3 s^{-1}) for gas phase reactions, the reaction with OH remains the main amide sink in the atmosphere.[172] In the aqueous aerosol phase, abstraction of an alkyl hydrogen atom is likely to remain the dominant initial reaction pathway for reactions of OH with amides. The loss of rotational freedom observed at the interface and the exposure of the alkyl group toward the particle surface may enhance the accessibility of alkyl hydrogens for abstraction by the radicals. Under such conditions, the interface reaction is likely to be faster than that occurring in the bulk. Saccharide molecules have also been detected in aerosols,[171] and the effect of surface partitioning on their heterogeneous oxidation has been discussed.[13] Alkyl substituted saccharides, however, may have drastically different behavior as they are more likely to be found at the interface and to lose their rotational freedom.

These findings are likely to apply to more abundant atmospheric compounds such as dicarboxylic acids. The OH radical reacts with dicarboxylic acids by abstraction of a hydrogen atom from the carbon chain. Upon addition of molecular oxygen, the reaction proceeds though Russell disproportionation or Bennett−Summers elimination as observed in the gas phase.[173] The final products are a mixture of alcohols and ketones. Scission of the carbon chain may lead to the formation of small volatile fragments. The final composition of the particle will be greatly dependent on the structure of the reacting acid. In the case of a multicomponent particle, molecules at the particle surface will be more likely to react with the OH radicals, making the overall chemical scheme very different from that of a system where the OH radicals react with all the solutes. Models trying to reproduce the chemical evolution of atmospheric aerosols must take such phenomena into account to accurately reproduce the heterogeneous chemistry.

■ ASSOCIATED CONTENT

Supporting Information

The Supporting Information is available free of charge at https://pubs.acs.org/doi/10.1021/acs.jpca.2c07419.

Time dependence of the interfacial and bulk concentrations, water radical pair distributions, OH scattering plot, glucose density profile, concentration dependence of the acetamide density profile, MGP carbon labeling, atom density profiles of urea and glucose, OH−propionamide radial pair distribution functions at low concentration, and radial pair distribution functions of OH with urea, acetamide, and propionamide (PDF)

■ AUTHOR INFORMATION

Corresponding Author

Fabien Goulay − *C. Eugene Bennett Department of Chemistry, West Virginia University, Morgantown, West Virginia 26506, United States*; orcid.org/0000-0002-7807-1023; Email: Fabien.Goulay@mail.wvu.edu

Author

Tadini Wenyika Masaya − *C. Eugene Bennett Department of Chemistry, West Virginia University, Morgantown, West Virginia 26506, United States*

Complete contact information is available at: https://pubs.acs.org/10.1021/acs.jpca.2c07419

Notes

The authors declare no competing financial interest.

■ ACKNOWLEDGMENTS

The authors are grateful to the National Science Foundation for its support of this work through Grant CHE-2106823. The authors also thank the West Virginia University High Performance Computing shared facility for providing computing resources and Dr. Blake Mertz and Nicholas Frazee for guidance on setting up, running, and analyzing of the MD simulations.

■ REFERENCES

(1) Vepsalainen, S.; Calderon, S. M.; Malila, J.; Prisle, N. L. Comparison of six approaches to predicting droplet activation of surface active aerosol - Part 1: moderately surface active organics. *Atmos. Chem. Phys.* **2022**, *22* (4), 2669−2687.

(2) Lowe, S. J.; Partridge, D. G.; Davies, J. F.; Wilson, K. R.; Topping, D.; Riipinen, I. Key drivers of cloud response to surface-active organics. *Nat. Commun.* **2019**, *10*, 5214.

(3) Nozière, B.; Baduel, C.; Jaffrezo, J. L. The dynamic surface tension of atmospheric aerosol surfactants reveals new aspects of cloud activation. *Nat. Commun.* **2014**, *5*, 3335.

(4) Ruehl, C. R.; Davies, J. F.; Wilson, K. R. An interfacial mechanism for cloud droplet formation on organic aerosols. *Science* **2016**, *351* (6280), 1447−1450.

(5) Bianchi, F.; Tröstl, J.; Junninen, H.; Frege, C.; Henne, S.; Hoyle, C. R.; Molteni, U.; Herrmann, E.; Adamov, A.; Bukowiecki, N.; et al. New particle formation in the free troposphere: A question of chemistry and timing. *Science* **2016**, *352*, 1109−1112.

(6) Lehtipalo, K.; Yan, C.; Dada, L.; Bianchi, F.; Xiao, M.; Wagner, R.; Stolzenburg, D.; Ahonen, L.; Amorim, A.; Baccarini, A.; Lehtipalo, K.; et al. Multicomponent new particle formation from sulfuric acid, ammonia, and biogenic vapors. *Sci. Adv.* **2018**, *4* (12), No. eaau536.

(7) Zhang, R.; Khalizov, A.; Wang, L.; Hu, M.; Xu, W. Nucleation and growth of nanoparticles in the atmosphere. *Chem. Rev.* **2012**, *112*, 1957−2011.

(8) Zhao, Z.; Kong, K.; Wang, S.; Zhou, Y.; Cheng, D.; Wang, W.; Zeng, X. C.; Li, H. Understanding Hygroscopic Nucleation of Sulfate Aerosols: Combination of Molecular Dynamics Simulation with Classical Nucleation Theory. *J. Phys. Chem. Lett.* **2019**, *10*, 1126−1132.

(9) Zeng, M. R.; Liu, C. L.; Wilson, K. R. Catalytic Coupling of Free Radical Oxidation and Electrophilic Chlorine Addition by Phase-Transfer Intermediates in Liquid Aerosols. *J. Phys. Chem. A* **2022**, *126* (19), 2959−2965.

(10) Zeng, M. R.; Wilson, K. R. Experimental evidence that halogen bonding catalyzes the heterogeneous chlorination of alkenes in submicron liquid droplets. *Chem. Sci.* **2021**, *12* (31), 10455−10466.

(11) Wilson, K. R.; Prophet, A. M.; Rovelli, G.; Willis, M. D.; Rapf, R. J.; Jacobs, M. I. A kinetic description of how interfaces accelerate reactions in micro-compartments. *Chem. Sci.* **2020**, *11* (32), 8533−8545.

(12) Martins-Costa, M. T. C.; Anglada, J. M.; Francisco, J. S.; Ruiz-Lopez, M. F. Photosensitization mechanisms at the air-water interface of aqueous aerosols. *Chem. Sci.* **2022**, *13* (9), 2624−2631.

(13) Fan, H.; Wenyika Masaya, T.; Goulay, F. Effect of surface-bulk partitioning on the heterogeneous oxidation of aqueous saccharide aerosols. *Phys. Chem. Chem. Phys.* **2019**, *21*, 2992−3001.

(14) Ruiz-Lopez, M. F.; Francisco, J. S.; Martins-Costa, M. T. C.; Anglada, J. M. Molecular reactions at aqueous interfaces. *Nat. Rev. Chem.* **2020**, *4* (9), 459−475.

(15) Lee, J. K.; Walker, K. L.; Han, H. S.; Kang, J.; Prinz, F. B.; Waymouth, R. M.; Nam, H. G.; Zare, R. N. Spontaneous generation of hydrogen peroxide from aqueous microdroplets. *Proc. Natl. Acad. Sci. U.S.A* **2019**, *116* (39), 19294−19298.

(16) Qian, Y. Q.; Brown, J. B.; Huang-Fu, Z. C.; Zhang, T.; Wang, H.; Wang, S. Y.; Dadap, J. I.; Rao, Y. In situ analysis of the bulk and

surface chemical compositions of organic aerosol particles. *Commun. Chem.* **2022**, *5* (1), 58.
(17) Nam, I.; Lee, J. K.; Nam, H. G.; Zare, R. N. Abiotic production of sugar phosphates and uridine ribonudeoside in aqueous microdroplets. *Proc. Natl. Acad. Sci. U.S.A* **2017**, *114* (47), 12396−12400.
(18) Kusaka, R.; Nihonyanagi, S.; Tahara, T. The photochemical reaction of phenol becomes ultrafast at the air-water interface. *Nat. Chem.* **2021**, *13*, 306−311.
(19) Ishiyama, T.; Tahara, T.; Morita, A. Why the Photochemical Reaction of Phenol Becomes Ultrafast at the Air-Water Interface: The Effect of Surface Hydration. *J. Am. Chem. Soc.* **2022**, *144*, 6321−6325.
(20) Zhu, C. Q.; Zeng, X. C.; Francisco, J. S.; Gladich, I. Hydration, Solvation, and Isomerization of Methylglyoxal at the Air/Water Interface: New Mechanistic Pathways. *J. Am. Chem. Soc.* **2020**, *142* (12), 5574−5582.
(21) Donaldson, D. J.; Valsaraj, K. T. Adsorption and Reaction of Trace Gas-Phase Organic Compounds on Atmospheric Water Film Surfaces: A Critical Review. *Environ. Sci. Technol.* **2010**, *44* (3), 865−873.
(22) Nissenson, P.; Knox, C. J. H.; Finlayson-Pitts, B. J.; Phillips, L. F.; Dabdub, D. Enhanced photolysis in aerosols: evidence for important surface effects. *Phys. Chem. Chem. Phys.* **2006**, *8* (40), 4700−4710.
(23) Wingen, L. M.; Moskun, A. C.; Johnson, S. N.; Thomas, J. L.; Roeselova, M.; Tobias, D. J.; Kleinman, M. T.; Finlayson-Pitts, B. J. Enhanced surface photochemistry in chloride-nitrate ion mixtures. *Phys. Chem. Chem. Phys.* **2008**, *10* (37), 5668−5677.
(24) Valsaraj, K. T. A Review of the Aqueous Aerosol Surface Chemistry in the Atmospheric Context. *Open J. Phys. Chem.* **2012**, *2*, 58−66.
(25) Ruiz-Lopez, M. F.; Martins-Costa, M. T. C. Disentangling reaction rate acceleration in microdroplets. *Phys. Chem. Chem. Phys.* **2022**, *24*, 29700.
(26) Shantz, N. C.; Leaitch, W. R.; Caffrey, P. F. Effects of organics of low solubility on the growth rate of cloud droplets. *J. Geophys. Res.: Atmos.* **2003**, *108*, 1−9.
(27) Asa-Awuku, A.; Miracolo, M. A.; Kroll, J. H.; Robinson, A. L.; Donahue, N. M. Mixing and phase partitioning of primary and secondary organic aerosols. *Geophys. Res. Lett.* **2009**, *36*, 1−5.
(28) Huang, Y.; Mahrt, F.; Xu, S.; Shiraiwa, M.; Zuend, A.; Bertram, A. K. Coexistence of three liquid phases in individual atmospheric aerosol particles. *Proc. Natl. Acad. Sci. U.S.A.* **2021**, *118*, No. e2102512118.
(29) Karadima, K. S.; Mavrantzas, V. G.; Pandis, S. N. Insights into the morphology of multicomponent organic and inorganic aerosols from molecular dynamics simulations. *Atmos. Chem. Phys.* **2019**, *19*, 5571−5587.
(30) Kucinski, T. M.; Dawson, J. N.; Freedman, M. A. Size-Dependent Liquid-Liquid Phase Separation in Atmospherically Relevant Complex Systems. *J. Phys. Chem. Lett.* **2019**, *10*, 6915−6920.
(31) Vaden, T. D.; Song, C.; Zaveri, R. A.; Imre, D.; Zelenyuk, A. Morphology of mixed primary and secondary organic particles and the adsorption of spectator organic gases during aerosol formation. *Proc. Natl. Acad. Sci. U.S.A* **2010**, *107*, 6658−6663.
(32) Fan, H. Y.; Goulay, F. Effect of Bulk Composition on the Heterogeneous Oxidation of Semi-Solid Atmospheric Aerosols. *Atmosphere* **2019**, *10* (12), 791.
(33) Pegram, L. M.; Record, M. T. Using surface tension data to predict differences in surface and bulk concentrations of nonelectrolytes in water. *J. Phys. Chem. C* **2009**, *113*, 2171−2174.
(34) Gerard, V.; Noziere, B.; Baduel, C.; Fine, L.; Frossard, A. A.; Cohen, R. C. Anionic, Cationic, and Nonionic Surfactants in Atmospheric Aerosols from the Baltic Coast at Asko, Sweden: Implications for Cloud Droplet Activation. *Environ. Sci. Technol.* **2016**, *50* (6), 2974−2982.
(35) Petters, S. S.; Petters, M. D. Surfactant effect on cloud condensation nuclei for two-component internally mixed aerosols. *J. Geophys. Res.-Atmos.* **2016**, *121* (4), 1878−1895.
(36) Kwan, V.; Consta, S. Bridging electrostatic properties between nanoscopic and microscopic highly charged droplets. *Chem. Phys. Lett.* **2020**, *746*, 137238.
(37) Kwan, V.; Consta, S. Molecular Characterization of the Surface Excess Charge Layer in Droplets. *J. Am. Soc. Mass Spectrom.* **2021**, *32* (1), 33−45.
(38) Frka, S.; Dautović, J.; Kozarac, Z.; Ćosović, B.; Hoffer, A.; Kiss, G. Surface-active substances in atmospheric aerosol: An electrochemical approach. *Tellus B: Chem. Phys. Meteorol.* **2022**, *64*, 18490.
(39) Bzdek, B. R.; Reid, J. P.; Malila, J.; Prisle, N. L. The surface tension of surfactant-containing, finite volume droplets. *Proc. Natl. Acad. Sci. U.S.A* **2020**, *117*, 8335−8343.
(40) Facchini, M. C.; Decesari, S.; Mircea, M.; Fuzzi, S.; Loglio, G. Surface tension of atmospheric wet aerosol and cloud/fog droplets in relation to their organic carbon content and chemical composition. *Atmos. Environ.* **2000**, *34*, 4853−4857.
(41) Sorjamaa, R.; Svenningsson, B.; Raatikainen, T.; Henning, S.; Bilde, M.; Laaksonen, A. The role of surfactants in Köhler theory reconsidered. *Atmos. Chem. Phys.* **2004**, *4*, 2107−2117.
(42) Harper, K.; Minofar, B.; Sierra-Hernandez, M. R.; Casillas-Ituarte, N. N.; Roeselova, M.; Allen, H. C. Surface Residence and Uptake of Methyl Chloride and Methyl Alcohol at the Air/Water Interface Studied by Vibrational Sum Frequency Spectroscopy and Molecular Dynamics. *J. Phys. Chem. A* **2009**, *113*, 2015−2024.
(43) Roy, S.; Biswas, B.; Mondal, J. A.; Singh, P. C. Heterodyne-Detected Vibrational Sum Frequency Generation Study of Air-Water-Fluoroalcohol Interface: Fluorocarbon Group-Induced Structural and Orientational Change of Interfacial Water. *J. Phys. Chem. C* **2018**, *122*, 26928−26933.
(44) Qian, Y. Q.; Deng, G. H.; Rao, Y. In Situ Spectroscopic Probing of Polarity and Molecular Configuration at Aerosol Particle Surfaces. *J. Phys. Chem. Lett.* **2020**, *11* (16), 6763−6771.
(45) Berger, R.; Lilach, Y.; Ayoub, Y.; Asscher, M. Photochemistry of molecules at confined environment: $CD_3Br/O/Ru(001)$ and CO_2 @ Ice. *Isr. J. Chem.* **2005**, *45* (1−2), 97−109.
(46) Harrison, I.; Polanyi, J. C.; Young, P. A. Photochemistry of absorbed molecules.3. Photodissociation and photodesorption of CH3Br adsorbed on LIF(001). *J. Chem. Phys.* **1988**, *89* (3), 1475−1497.
(47) Habartová, A.; Valsaraj, K. T.; Roeselová, M. Molecular dynamics simulations of small halogenated organics at the air-water interface: Implications in water treatment and atmospheric chemistry. *J. Phys. Chem. A* **2013**, *117*, 9205−9215.
(48) Pašalić, H.; Roeselová, M.; Lischka, H. Methyl and pentyl chloride in a microhydrated environment and at the liquid water-vapor interface: A theoretical study. *J. Phys. Chem. B* **2011**, *115*, 1807−1816.
(49) Benjamin, I. Structure, thermodynamics, and dynamics of the liquid/vapor interface of water/dimethylsulfoxide mixtures. *J. Chem. Phys.* **1999**, *110* (16), 8070−8079.
(50) Fabian, B.; Horvai, G.; Sega, M.; Jedlovszky, P. Single Particle Dynamics at the Liquid-Liquid Interface. Molecular Dynamics Simulation Study of the Water-CCl4 System. *J. Phys. Chem. C* **2020**, *124* (3), 2039−2049.
(51) Kuhn, H.; Rehage, H. Molecular orientation of monododecyl pentaethylene glycol at water/air and water/oil interfaces. A molecular dynamics computer simulation study. *Colloid Polym. Sci.* **2000**, *278* (2), 114−118.
(52) Makowski, M. J.; Stern, A. C.; Hemminger, J. C.; Tobias, D. J. Orientation and Structure of Acetonitrile in Water at the Liquid-Vapor Interface: A Molecular Dynamics Simulation Study. *J. Phys. Chem. C* **2016**, *120* (31), 17555−17563.
(53) Mountain, R. D. Molecular dynamics study of thin water-acetonitrile films. *J. Phys. Chem. B* **2001**, *105* (28), 6556−6561.
(54) Strazdaite, S.; Versluis, J.; Ottosson, N.; Bakker, H. J. Orientation of Methylguanidinium Ions at the Water-Air Interface. *J. Phys. Chem. C* **2017**, *121* (42), 23398−23405.

(55) Thomas, J. L.; Roeselova, M.; Dang, L. X.; Tobias, D. J. Molecular dynamics simulations of the solution-air interface of aqueous sodium nitrate. *J. Phys. Chem. A* **2007**, *111* (16), 3091−3098.
(56) Zhong, J.; Zhang, W. N.; Wu, S.; An, T. C.; Francisco, J. S. Molecular Interaction and Orientation of HOCl on Aqueous and Ice Surfaces. *J. Am. Chem. Soc.* **2020**, *142* (41), 17329−17333.
(57) Jonsson, A. L.; Roberts, M. A. J.; Kiappes, J. L.; Scott, K. A. Essential chemistry for biochemists. *Essays Biochem.* **2017**, *61*, 401−427.
(58) Monroe, J. I.; Jiao, S.; Davis, R. J.; Brown, D. R.; Katz, L. E.; Shell, M. S. Affinity of small-molecule solutes to hydrophobic, hydrophilic, and chemically patterned interfaces in aqueous solution. *Proc. Natl. Acad. Sci. U.S.A.* **2021**, *118*, e2020205118.
(59) Wang, Y. P.; Ren, K. Z.; Liu, S. L. The joint effect of surface polarity and concentration on the structure and dynamics of acetonitrile solution: a molecular dynamics simulation study. *Phys. Chem. Chem. Phys.* **2020**, *22* (18), 10322−10334.
(60) Klijn, J. E.; Engberts, J. Organic chemistry - Fast reactions 'on water'. *Nature* **2005**, *435* (7043), 746−747.
(61) Litwinienko, G.; Ingold, K. U. Solvent effects on the rates and mechanisms of reaction of phenols with free radicals. *Acc. Chem. Res.* **2007**, *40*, 222−230.
(62) Mitroka, S.; Zimmeck, S.; Troya, D.; Tanko, J. M. How solvent modulates hydroxyl radical reactivity in hydrogen atom abstractions. *J. Am. Chem. Soc.* **2010**, *132*, 2907−2913.
(63) Codorniu-Hernández, E.; Kusalik, P. G. Mobility mechanism of hydroxyl radicals in aqueous solution via hydrogen transfer. *J. Am. Chem. Soc.* **2012**, *134*, 532−538.
(64) Wick, C. D.; Xantheas, S. S. Computational Investigation of the First Solvation Shell Structure of Interfacial and Bulk Aqueous Chloride and Iodide Ions. *J. Phys. Chem. B* **2009**, *113*, 4141−4146.
(65) Long, J. A.Hydrophobic Hydration and Aggregation in Aqueous Solutions. Ph.D., Purdue University, West Lafayette, IN, 2017.
(66) Conti Nibali, V.; Pezzotti, S.; Sebastiani, F.; Galimberti, D. R.; Schwaab, G.; Heyden, M.; Gaigeot, M. P.; Havenith, M. Wrapping up Hydrophobic Hydration: Locality Matters. *J. Phys. Chem. Lett.* **2020**, *11*, 4809−4816.
(67) Mountain, R. D. Solvation structure of ions in water. *Int. J. Thermophys.* **2007**, *28*, 536−543.
(68) Burkholder, J. B.; Abbatt, J. P. D.; Barnes, I.; Roberts, J. M.; Melamed, M. L.; Ammann, M.; Bertram, A. K.; Cappa, C. D.; Carlton, A. G.; Carpenter, L. J.; et al. The Essential Role for Laboratory Studies in Atmospheric Chemistry. *Environ. Sci. Technol.* **2017**, *51*, 2519−2528.
(69) Roeselová, M.; Vieceli, J.; Dang, L. X.; Garrett, B. C.; Tobias, D. J. Hydroxyl radical at the air-water interface. *J. Am. Chem. Soc.* **2004**, *126*, 16308−16309.
(70) Vacha, R.; Slavicek, P.; Mucha, M.; Finlayson-Pitts, B. J.; Jungwirth, P. Adsorption of Atmospherically Relevant Gases at the Air/Water Interface: Free Energy Profiles of Aqueous Solvation of N_2, O_2, O_3, OH, H_2O, HO_2, and H_2O_2. *J. Phys. Chem. A* **2004**, *108*, 11573−11579.
(71) Du, S.; Francisco, J. S. Interaction between OH radical and the water interface. *J. Phys. Chem. A* **2008**, *112* (21), 4826−4835.
(72) Martins-Costa, M. T. C.; Anglada, J. M.; Francisco, J. S.; Ruiz-Lopez, M. F. Reactivity of atmospherically relevant small radicals at the air-water interface. *Angew. Chem., Int. Ed.* **2012**, *51*, 5413−5417.
(73) Apostolidou, C. OH radical in water from ab initio molecular dynamics simulation employing hybrid functionals. *J. Chem. Phys.* **2019**, *151* (6), 064111.
(74) Apostolidou, C. Vibrational Spectra of the OH Radical in Water: Ab Initio Molecular Dynamics Simulations and Quantum Chemical Calculations Using Hybrid Functionals. *Adv. Theory Simul.* **2020**, *3* (12), 2000174.
(75) Houle, F. A.; Wiegel, A. A.; Wilson, K. R. Changes in Reactivity as Chemistry Becomes Confined to an Interface. The Case of Free Radical Oxidation of C30H62 Alkane by OH. *J. Phys. Chem. Lett.* **2018**, *9* (5), 1053−1057.
(76) Wiegel, A. A.; Wilson, K. R.; Hinsberg, W. D.; Houle, F. A. Stochastic methods for aerosol chemistry: a compact molecular description of functionalization and fragmentation in the heterogeneous oxidation of squalane aerosol by OH radicals. *Phys. Chem. Chem. Phys.* **2015**, *17* (6), 4398−4411.
(77) Fan, H. Y.; Tinsley, M. R.; Goulay, F. Effect of Relative Humidity on the OH-Initiated Heterogeneous Oxidation of Monosaccharide Nanoparticles. *J. Phys. Chem. A* **2015**, *119* (45), 11182−11190.
(78) Collins, D. B.; Grassian, V. H.Gase-Liquid Interfaces in the Atmosphere: Impacts, Complexity, and Challenges. In *Physical Chemistry of Gas−Liquid Interfaces*; Faust, J., House, J. E., Eds.; Elsevier, 2018; Chapter 10, pp 271−313.
(79) Hadizadeh, M. H.; Yang, L.; Fang, G.; Qiu, Z.; Li, Z. The mobility and solvation structure of a hydroxyl radical in a water nanodroplet: a Born-Oppenheimer molecular dynamics study. *Phys. Chem. Chem. Phys.* **2021**, *23*, 14628−14635.
(80) Vassilev, P.; Louwerse, M. J.; Baerends, E. J. Ab initio molecular dynamics simulation of the OH center dot radical in liquid water. *Chem. Phys. Lett.* **2004**, *398* (1−3), 212−216.
(81) VandeVondele, J.; Sprik, M. A molecular dynamics study of the hydroxyl radical in solution applying self-interaction-corrected density functional methods. *Phys. Chem. Chem. Phys.* **2005**, *7* (7), 1363−1367.
(82) Codorniu-Hernandez, E.; Kusalik, P. G. Insights into the Solvation and Mobility of the Hydroxyl Radical in Aqueous Solution. *J. Chem. Theory Comput.* **2011**, *7* (11), 3725−3732.
(83) Rana, B.; Herbert, J. M. Hidden Hemibonding in the Aqueous Hydroxyl Radical. *J. Phys. Chem. Lett.* **2021**, *12* (33), 8053−8060.
(84) Campo, M. G.; Grigera, J. R. Classical molecular-dynamics simulation of the hydroxyl radical in water. *J. Chem. Phys.* **2005**, *123*, 084507.
(85) Swiatla-Wojcik, D.; Szala-Bilnik, J. Mechanism of OH radical hydration: A comparative computational study of liquid and supercritical solvent. *J. Chem. Phys.* **2012**, *136* (6), 064510.
(86) Dudik, J. M.; Johnson, C. R.; Asher, S. A. UV resonance Raman studies of acetone, acetamide, and N-methylacetamide- Model for the peptide-bond. *J. Phys. Chem.* **1985**, *89* (18), 3805−3814.
(87) Knudsen, R.; Sala, O.; Hase, Y. A low temperature matrix isolation infrared study of acetamides. I. Acetamide and some deuterated derivatives. *J. Mol. Struct.* **1994**, *321*, 187−195.
(88) Chen, X. G.; Schweitzer-Stenner, R.; Asher, S. A.; Mirkin, N. G.; Krimm, S. Vibrational assigments of trans-N-methylacetamide and some of its deuterated isotopomers from band decomposition of IR, visible, and resonance Raman spectra. *J. Phys. Chem.* **1995**, *99*, 3074−3083.
(89) Schweitzer-Stenner, R.; Sieler, G.; Mirkin, N. G.; Krimm, S. Intermolecular coupling in liquid and crystalline states of trans-N-methylacetamide investigated by polarized raman and FT-IR spectroscopies. *J. Phys. Chem. A* **1998**, *102*, 118−127.
(90) Woutersen, S.; Mu, Y.; Stock, G.; Hamm, P. Hydrogen-bond lifetime measured by time-resolved 2D-IR spectroscopy: N-methylacetamide in methanol. *Chem. Phys.* **2001**, *266*, 137−147.
(91) Barthel, J.; Buchner, R.; Wurm, B. The dynamics of liquid formamide, N-methylformamide, N,N-dimethylformamide, and N,N-dimethylacetamide. A dielectric relaxation study. *J. Mol. Liq.* **2002**, *98−99*, 51−69.
(92) Xu, Z.; Li, H.; Wang, C.; Wu, T.; Han, S. Is the blue shift of C-H vibration in DMF-water mixture mainly caused by C-H···O interaction? *Chem. Phys. Lett.* **2004**, *394*, 405−409.
(93) Zhang, R.; Li, H.; Lei, Y.; Han, S. Structures and interactions in N-methylacetamide-water mixtures studied by IR spectra and density functional theory. *J. Mol. Struct.* **2004**, *693*, 17−25.
(94) Zhang, R.; Li, H.; Lei, Y.; Han, S. All-atom molecular dynamic simulations and relative NMR spectra study of weak C-H···O contacts in amide-water systems. *J. Phys. Chem. B* **2005**, *109*, 7482−7487.
(95) DeCamp, M. F.; DeFlores, L.; McCracken, J. M.; Tokmakoff, A.; Kwac, K.; Cho, M. Amide I vibrational dynamics of N-

methylacetamide in polar solvents: The role of electrostatic interactions. *J. Phys. Chem. B* **2005**, *109*, 11016−11026.
(96) Fujitake, M.; Kubota, Y.; Ohashi, N. Fourier transform microwave spectroscopy of N,N-dimethylacetamide. *J. Mol. Spectrosc.* **2006**, *236*, 97−109.
(97) Albrecht, M.; Rice, C. A.; Suhm, M. A. Elementary peptide motifs in the gas phase: FTIR aggregation study of formamide, acetamide, N-methylformamide, and N-methylacetamide. *J. Phys. Chem. A* **2008**, *112*, 7530−7542.
(98) Zhou, Y.; Deng, G.; Zheng, Y. Z.; Xu, J.; Ashraf, H.; Yu, Z. W. Evidences for Cooperative Resonance-Assisted Hydrogen Bonds in Protein Secondary Structure Analogs. *Sci. Rep.* **2016**, *6*, 36932.
(99) Forsting, T.; Gottschalk, H. C.; Hartwig, B.; Mons, M.; Suhm, M. A. Correcting the record: The dimers and trimers of: Trans-N -methylacetamide. *Phys. Chem. Chem. Phys.* **2017**, *19*, 10727−10737.
(100) Salamatova, E.; Cunha, A. V.; Bloem, R.; Roeters, S. J.; Woutersen, S.; Jansen, T. L. C.; Pshenichnikov, M. S. Hydrophobic Collapse in N -Methylacetamide-Water Mixtures. *J. Phys. Chem. A* **2018**, *122*, 2468−2478.
(101) Jorgensen, W. L.; Gao, J. Cis-Trans Energy Difference for the Peptide Bond in the Gas Phase and in Aqueous Solution. *J. Am. Chem. Soc.* **1988**, *110*, 4212−4216.
(102) Almeida, G. G.; Cordeiro, J. M. M. A Monte Carlo revisiting of N-methylformamide and acetone. *J. Braz. Chem. Soc.* **2011**, *22*, 2178−2185.
(103) Chalaris, M.; Samios, J. Systematic molecular dynamics studies of liquid N,N-dimethylformamide using optimized rigid force fields: Investigation of the thermodynamic, structural, transport and dynamic properties. *J. Chem. Phys.* **2000**, *112*, 8581−8594.
(104) Kwac, K.; Cho, M. Molecular dynamics simulation study of N-methylacetamide in water. II. Two-dimensional infrared pump-probe spectra. *J. Chem. Phys.* **2003**, *119*, 2256−2263.
(105) Lei, Y.; Li, H.; Pan, H.; Han, S. Structures and Hydrogen Bonding Analysis of N, N -Dimethylformamide and. *J. Phys. Chem. A* **2003**, *107*, 1574−1583.
(106) Gaigeot, M. P.; Vuilleumier, R.; Sprik, M.; Borgis, D. Infrared spectroscopy of N-methylacetamide revisited by ab initio molecular dynamics simulations. *J. Chem. Theory Comput.* **2005**, *1*, 772−789.
(107) Mennucci, B.; Martínez, J. M. How to model solvation of peptides? Insights from a quantum-mechanical and molecular dynamics study of N-methylacetamide. 1. Geometries, infrared, and ultraviolet spectra in water. *J. Phys. Chem. B* **2005**, *109*, 9818−9829.
(108) Aparicio-Martínez, S.; Balbuena, P. B. On the properties of aqueous amide solutions through classical molecular dynamics simulations. *Mol. Simul.* **2007**, *33*, 925−938.
(109) Heyda, J.; Vincent, J. C.; Tobias, D. J.; Dzubiella, J.; Jungwirth, P. Ion specificity at the peptide bond: molecular dynamics simulations of N-methylacetamide in aqueous salt solutions. *J. Phys. Chem. B* **2010**, *114*, 1213−1220.
(110) Watanabe, H.; Yamaguchi, S.; Sen, S.; Morita, A.; Tahara, T. "Half-hydration" at the air/water interface revealed by heterodyne-detected electronic sum frequency generation spectroscopy, polarization second harmonic generation, and molecular dynamics simulation. *J. Chem. Phys.* **2010**, *132* (14), 144701.
(111) Biswas, A.; Mallik, B. S. Structure and stretching dynamics of water molecules around an amphiphilic amide from FPMD simulations: A case study of N,N-dimethylformamide. *J. Mol. Liq.* **2020**, *302*, 112524.
(112) Chen, W.; Karde, V.; Cheng, T. N. H.; Ramli, S. S.; Heng, J. Y. Y. Surface hydrophobicity: effect of alkyl chain length and network homogeneity. *Front. Chem. Sci. Eng.* **2021**, *15*, 90−98.
(113) Gao, Y.; Duan, L.; Guan, S.; Gao, G.; Cheng, Y.; Ren, X.; Wang, Y. The effect of hydrophobic alkyl chain length on the mechanical properties of latex particle hydrogels. *RSC Adv.* **2017**, *7*, 44673−44679.
(114) Jackson, M. B. The Hydrophobic Effect in Solute Partitioning and Interfacial Tension. *Sci. Rep.* **2016**, *6*, 19265.
(115) Yun, H.; Choi, Y. W.; Kim, N. J.; Sohn, D. Physicochemical properties of phosphatidylcholine (PC) monolayers with different alkyl chains, at the air/water interface. *Bull. Korean Chem. Soc.* **2003**, *24*, 377−383.
(116) Brady, J. W.; Ha, S. N. Molecular dynamics simulation of the aqueous solvation of sugars. *Adv. Exp. Med. Biol.* **1991**, *302*, 739−751.
(117) Brady, J. W.Molecular dynamics simulations of carbohydrate solvation. In *Modern Methods for Multidimensional Dynamics Computations in Chemistry*; Thompson, D. L., Ed.; World Scientific, 1998; pp 384−400, DOI: 10.1142/9789812812162_0011.
(118) Engelsen, S.; Monteiro, C.; Herve de Penhoat, C.; Perez, S. The diluted aqueous solvation of carbohydrates as inferred from molecular dynamics simulations and NMR spectroscopy. *Biophys. Chem.* **2001**, *93*, 103−127.
(119) Kirschner, K. N.; Woods, R. J. Solvent interactions determine carbohydrate conformation. *Proc. Natl. Acad. Sci. U.S.A* **2001**, *98*, 10541−10545.
(120) Pereira, C. S.; Kony, D.; Baron, R.; Müller, M.; Van Gunsteren, W. F.; Hünenberger, P. H. Conformational and dynamical properties of disaccharides in water: A molecular dynamics study. *Biophys. J.* **2006**, *90*, 4337−4344.
(121) Ruda, A.; Widmalm, G.; Wohlert, J. O-methylation in carbohydrates: An NMR and MD simulation study with application to methylcellulose. *J. Phys. Chem. B* **2021**, *125*, 11967−11979.
(122) Palivec, V.; Johannessen, C.; Kaminský, J.; Martinez- Seara, H. Use of Raman and Raman optical activity to extract atomistic details of saccharides in aqueous solution. *PLoS Comput. Biol.* **2022**, *18*, e1009678.
(123) Rovelli, G.; Jacobs, M. I.; Willis, M. D.; Rapf, R. J.; Prophet, A. M.; Wilson, K. R. A critical analysis of electrospray techniques for the determination of accelerated rates and mechanisms of chemical reactions in droplets. *Chem. Sci.* **2020**, *11* (48), 13026−13043.
(124) Jacobs, M. I.; Davis, R. D.; Rapf, R. J.; Wilson, K. R. Studying Chemistry in Micro-compartments by Separating Droplet Generation from Ionization. *J. Am. Soc. Mass Spectrom.* **2019**, *30* (2), 339−343.
(125) Hayon, E.; Ibata, T.; Lichtin, N. N.; Simic, M. Sites of attach of hydroxyl radicals on amides in aqueous solution. *J. Am. Chem. Soc.* **1970**, *92* (13), 3898−3903.
(126) Madden, K. P.; Fessenden, R. W. ESR study of the attack of photolytically produced hydroxyl radicals on alpha-methyl-D-glucopyranoside in aqueous solution. *J. Am. Chem. Soc.* **1982**, *104* (9), 2578−2581.
(127) Schuchmann, M. N.; von Sonntag, C. Radiation-chemistry of carbohydrates. Part 14. Hydroxyl radical induced oxidation of D-glucose in oxygenated aqueous-solution. *J. Chem. Soc., Perkin Trans. 2* **1977**, No. 14, 1958−1963.
(128) Karpel Vel Leitner, N.; Berger, P.; Legube, B. Oxidation of amino groups by hydroxyl radicals in relation to the oxidation degree of the alpha-carbon. *Environ. Sci. Technol.* **2002**, *36* (14), 3083−3089.
(129) Yuet, P. K.; Blankschtein, D. Molecular dynamics simulation study of water surfaces: Comparison of flexible water models. *J. Phys. Chem. B* **2010**, *114*, 13786−13795.
(130) Fan, Y.; Chen, X.; Yang, L.; Cremer, P.; Gao, Y. Q. On the structure of water at the aqueous/air interface. *J. Phys. Chem. B* **2009**, *113*, 11672−11679.
(131) Jungwirth, P.; Tobias, D. J. Ions at the Air/Water Interface. *J. Phys. Chem. B* **2002**, *106*, 6361−6373.
(132) MacKerell, A. D.; Bashford, D.; Bellott, M.; Dunbrack, R. L.; Evanseck, J. D.; Field, M. J.; Fischer, S.; Gao, J.; Guo, H.; Ha, S.; et al. All-atom empirical potential for molecular modeling and dynamics studies of proteins. *J. Phys. Chem. B* **1998**, *102*, 3586−3616.
(133) Jorgensen, W. L.; Chandrasekhar, J.; Madura, J. D.; Impey, R. W.; Klein, M. L. Comparison of simple potential functions for simulating liquid water. *J. Chem. Phys.* **1983**, *79*, 926−935.
(134) Svishchev, I. M.; Plugatyr, A. Y. Hydroxyl radical in aqueous solution: Computer simulation. *J. Phys. Chem. B* **2005**, *109*, 4123−4128.
(135) Guvench, O.; Greene, S. N.; Kamath, G.; Brady, J. W.; Venable, R. M.; Pastor, R. W.; Mackerell, A. D. Additive empirical force field for hexopyranose monosaccharides. *J. Comput. Chem.* **2008**, *29*, 2543−2564.

(136) Hatcher, E. R.; Guvench, O.; MacKerell, A. D. CHARMM Additive All-Atom Force Field for Acyclic Polyalcohols, Acyclic Carbohydrates, and Inositol. *J. Chem. Theory Comput.* **2009**, *5*, 1315−1327.

(137) Darden, T.; York, D.; Pedersen, L. Particle mesh Ewald: An N·log(N) method for Ewald sums in large systems. *J. Chem. Phys.* **1993**, *98*, 10089−10092.

(138) Iupinov, A.Implementation of the Particle Mesh Ewald Method on a GPU. Master's Thesis, Royal Institute of Technology, Stockholm, Sweden, 2016.

(139) Phillips, J. C.; Hardy, D. J.; Maia, J. D. C.; Stone, J. E.; Ribeiro, J. V.; Bernardi, R. C.; Buch, R.; Fiorin, G.; Hénin, J.; Jiang, W.; et al. Scalable molecular dynamics on CPU and GPU architectures with NAMD. *J. Chem. Phys.* **2020**, *153*, 044130.

(140) Martinez, L.; Andrade, R.; Birgin, E. G.; Martinez, J. M. PACKMOL: A Package for Building Initial Configurations for Molecular Dynamics Simulations. *J. Comput. Chem.* **2009**, *30* (13), 2157−2164.

(141) Humphrey, W.; Dalke, A.; Schulten, K. Sartorius products. *J. Mol. Graph.* **1996**, *14*, 33−38.

(142) Grønbech-Jensen, N.; Farago, O. Constant pressure and temperature discrete-time Langevin molecular dynamics. *J. Chem. Phys.* **2014**, *141*, 194108.

(143) Wang, X.; Chen, C.; Binder, K.; Kuhn, U.; Pöschl, U.; Su, H.; Cheng, Y. Molecular dynamics simulation of the surface tension of aqueous sodium chloride: From dilute to highly supersaturated solutions and molten salt. *Atmos. Chem. Phys.* **2018**, *18*, 17077−17086.

(144) Giorgino, T. Computing 1-D atomic densities in macromolecular simulations: The density profile tool for VMD. *Comput. Phys. Commun.* **2014**, *185*, 317−322.

(145) Levine, B. G.; Stone, J. E.; Kohlmeyer, A. Fast analysis of molecular dynamics trajectories with graphics processing units-Radial distribution function histogramming. *J. Comput. Phys.* **2011**, *230*, 3556−3569.

(146) Pranami, G.; Lamm, M. H. Estimating Error in Diffusion Coefficients Derived from Molecular Dynamics Simulations. *J. Chem. Theory Comput.* **2015**, *11*, 4586−4592.

(147) Haile, J. M.*Molecular Dynamics Simulation: Elementary Methods*; Wiley: New York, 1997.

(148) Wang, J. M.; Hou, T. J. Application of Molecular Dynamics Simulations in Molecular Property Prediction. 1. Density and Heat of Vaporization. *J. Chem. Theory Comput.* **2011**, *7* (7), 2151−2165.

(149) van der Spoel, D.; van Maaren, P. J.; Berendsen, H. J. C. A systematic study of water models for molecular simulation: Derivation of water models optimized for use with a reaction field. *J. Chem. Phys.* **1998**, *108* (24), 10220−10230.

(150) Mark, P.; Nilsson, L. Structure and dynamics of the TIP3P, SPC, and SPC/E water models at 298 K. *J. Phys. Chem. A* **2001**, *105*, 9954−9960.

(151) Mahoney, M. W.; Jorgensen, W. L. Diffusion constant of the TIP5P model of liquid water. *J. Chem. Phys.* **2001**, *114*, 363−366.

(152) Wu, Y.; Tepper, H. L.; Voth, G. A. Flexible simple point-charge water model with improved liquid-state properties. *J. Chem. Phys.* **2006**, *124*, 024503.

(153) Vega, C.; De Miguel, E. Surface tension of the most popular models of water by using the test-area simulation method. *J. Chem. Phys.* **2007**, *126*, 154707.

(154) Wang, J.; Hou, T. Application of molecular dynamics simulations in molecular property prediction II: diffusion coefficient. *J. Comput. Chem.* **2011**, *32*, 3505−3519.

(155) Leontyev, I. V.; Stuchebrukhov, A. A. Polarizable Mean-Field Model of Water for Biological Simulations with Amber and Charmm force fields. *J. Chem. Theory Comput.* **2012**, *8*, 3207−3216.

(156) Chen, Y.-D.; Li, A.; Huang-Te; Wang, Y.-S.; Chao, S. D. Molecular dynamics simulations of liquid water structure and diffusivity. *Chin. J. Phys.* **2013**, *51* (6), 1218−1229.

(157) Yu, W.; Lopes, P. E. M.; Roux, B.; MacKerell, A. D. Six-site polarizable model of water based on the classical Drude oscillator. *J. Chem. Phys.* **2013**, *138*, 034508.

(158) Braun, D.; Boresch, S.; Steinhauser, O. Transport and dielectric properties of water and the influence of coarse-graining: Comparing BMW, SPC/E, and TIP3P models. *J. Chem. Phys.* **2014**, *140*, 064107.

(159) Holz, M.; Heil, S. R.; Sacco, A. Temperature-dependent self-diffusion coefficients of water and six selected molecular liquids for calibration in accurate 1H NMR PFG measurements. *Phys. Chem. Chem. Phys.* **2000**, *2*, 4740−4742.

(160) Price, D. J.; Brooks, C. L. A modified TIP3P water potential for simulation with Ewald summation. *J. Chem. Phys.* **2004**, *121*, 10096−10103.

(161) De Kock, M. B.; Azim, S.; Kassier, G. H.; Miller, R. J. D. Determining the radial distribution function of water using electron scattering: A key to solution phase chemistry. *J. Chem. Phys.* **2020**, *153*, 194504.

(162) Soper, A. K.; Phillips, M. G. A new determination of the structure of water at 25°C. *Chem. Phys.* **1986**, *107*, 47−60.

(163) Campo, M. G.; Grigera, J. R. Classical molecular-dynamics simulation of the hydroxyl radical in water. *J. Chem. Phys.* **2005**, *123* (8), 084507.

(164) Aguilar-Pineda, J. A.; Mendez-Maldonado, G. A.; Nunez-Rojas, E.; Alejandre, J. Parametrisation of a force field of acetamide for simulations of the liquid phase. *Mol. Phys.* **2015**, *113* (17−18), 2716−2724.

(165) Halonen, S.; Kangas, T.; Haataja, M.; Lassi, U. Urea-Water-Solution Properties: Density, Viscosity, and Surface Tension in an Under-Saturated Solution. *Emiss. Control Sci. Technol.* **2017**, *3*, 161−170.

(166) Lee, J. Y.; Hildemann, L. M. Surface tension of solutions containing dicarboxylic acids with ammonium sulfate, D-glucose, or humic acid. *J. Aerosol. Sci.* **2013**, *64*, 94−102.

(167) Julin, J.; Shiraiwa, M.; Miles, R. E. H.; Reid, J. P.; Pöschl, U.; Riipinen, I. Mass accommodation of water: Bridging the gap between molecular dynamics simulations and kinetic condensation models. *J. Phys. Chem. A* **2013**, *117*, 410−420.

(168) Lee, W. C.; Ronghe, A.; Villalobos, L. F.; Huang, S. Q.; Dakhchoune, M.; Mensi, M.; Hsu, K. J.; Ayappa, K. G.; Agrawal, K. V. Enhanced Water Evaporation from A-Scale Graphene Nanopores. *ACS Nano* **2022**, *16* (9), 15382−15396.

(169) Tabazadeh, A.; Yokelson, R. J.; Singh, H. B.; Hobbs, P. V.; Crawford, J. H.; Iraci, L. T. Heterogeneous chemistry involving methanol in tropospheric clouds. *Geophys. Res. Lett.* **2004**, *31*, 2−5.

(170) Booyens, W.; Van Zyl, P. G.; Beukes, J. P.; Ruiz-Jimenez, J.; Kopperi, M.; Riekkola, M. L.; Vakkari, V.; Josipovic, M.; Kulmala, M.; Laakso, L. Characterising Particulate Organic Nitrogen at A Savannah-Grassland Region in South Africa. *Atmosphere* **2019**, *10* (9), 492.

(171) Wan, E. C. H.; Yu, J. Z. Analysis of sugars and sugar polyols in atmospheric aerosols by chloride attachment in liquid chromatography/negative ion electrospray mass spectrometry. *Environ. Sci. Technol.* **2007**, *41* (7), 2459−2466.

(172) Borduas, N.; da Silva, G.; Murphy, J. G.; Abbatt, J. P. D. Experimental and Theoretical Understanding of the Gas Phase Oxidation of Atmospheric Amides with OH Radicals: Kinetics, Products, and Mechanisms. *J. Phys. Chem. A* **2015**, *119* (19), 4298−4308.

(173) Lam, H. K.; Shum, S. M.; Davies, J. F.; Song, M.; Zuend, A.; Chan, M. N. Effects of inorganic salts on the heterogeneous OH oxidation of organic compounds: insights from methylglutaric acid-ammonium sulfate. *Atmos. Chem. Phys.* **2019**, *19* (14), 9581−9593.

https://doi.org/10.1021/acs.jpca.2c07419
J. Phys. Chem. A 2023, 127, 751−764